

Determination of cluster distances from Chandra imaging spectroscopy and Sunyaev-Zeldovich Effect measurements: I - Analysis methods and initial results

Massimiliano Bonamente^{1,2}, Marshall K. Joy², John E. Carlstrom^{3,4} and Samuel J. LaRoque³

¹*Department of Physics, University of Alabama, Huntsville, AL*

²*NASA Marshall Space Flight Center, Huntsville, AL*

³*Department of Astronomy and Astrophysics, University of Chicago, Chicago, IL 60637*

⁴*Center for Cosmological Physics, Department of Physics, Enrico Fermi Institute, University of Chicago, Chicago, IL 60637*

ABSTRACT

X-ray and Sunyaev-Zeldovich Effect data can be combined to determine the distance to galaxy clusters. High-resolution X-ray data are now available from the Chandra Observatory, which provides both spatial and spectral information, and interferometric radio measurements of the Sunyaev-Zeldovich Effect are available from the BIMA and OVRO arrays. We introduce a Monte Carlo Markov chain procedure for the joint analysis of X-ray and Sunyaev-Zeldovich Effect data. The advantages of this method are the high computational efficiency and the ability to measure the full probability distribution of all parameters of interest, such as the spatial and spectral properties of the cluster gas and the cluster distance. We apply this technique to the Chandra X-ray data and the OVRO radio data for the galaxy cluster Abell 611. Comparisons with traditional likelihood-ratio methods reveal the robustness of the method. This method will be used in a follow-up paper to determine the distance of a large sample of galaxy clusters for which high-resolution Chandra X-ray and BIMA/OVRO radio data are available.

Subject headings: cosmic microwave background – cosmology:observations – distance scale – galaxies:clusters:general – techniques:interferometric – methods:statistical

1. Introduction

Analysis of the Sunyaev-Zeldovich Effect (SZE) and X-ray data provides a unique method of directly determining distances of galaxy clusters. Clusters of galaxies contain very

hot plasma ($K_B T_e \sim 2\text{-}20$ keV) which scatters the cosmic microwave background radiation (CMB). On average, this inverse Compton scattering boosts the energy of the CMB photons, causing a small distortion in the CMB spectrum (Sunyaev and Zeldovich 1970,1972).

The SZE is proportional to the integrated pressure along the line of sight, $\Delta T \propto \int n_e T_e dl$, where n_e and T_e are respectively the electron density and electron temperature of the cluster plasma. The thermal X-ray emission from the same plasma has a different dependence on the density, $S_x \propto \int n_e^2 \Lambda_{eH} dl$, where Λ_{eH} is the X-ray cooling function. Making assumptions on the distribution of the plasma (e.g., a β profile) and taking advantage of the different dependence on n_e , SZE and X-ray observations can be combined to determine the distance to galaxy clusters, as shown in section 3 (Birkinshaw 1999; Reese et al. 2002; Grainge et al. 2002; Myers et al. 1997; Mason, Myers and Readhead 2001). These cluster distances can be combined with redshift measurements to determine the value of the Hubble constant. Reese et al. (2002) used a sample of 18 clusters to constrain the value of the Hubble constant to $H_0 = 60 \pm_{22}^{17}$ km s⁻¹ Mpc⁻¹ for an $\Omega_M=0.3$, $\Omega_\Lambda=0.7$ cosmology.

A Monte Carlo Markov chain (MCMC) procedure is here introduced for the first time for the joint analysis of SZE and X-ray data. This method is tested on the galaxy cluster Abell 611 which has SZE data from the Owens Valley Radio Observatory (OVRO) and X-ray data from the *Chandra* X-ray Observatory. In a subsequent paper we will apply this technique to a sample of ~ 40 clusters which have *Chandra* X-ray data and SZE data from OVRO and the Berkeley-Illinois-Maryland Association (BIMA) observatory.

2. Data

2.1. *Chandra* X-ray data

The Advanced CCD Imaging Spectrometer (ACIS) aboard the *Chandra* X-ray Observatory provides high angular resolution (half-power radius ~ 0.5 arcsec) and good spectral resolution (50-300 eV FWHM) in the $\sim 0.3 - 10$ keV energy range. We use the following steps to reduce the raw (Level 1) *Chandra* data:

- (a) We use the "acis_process_events" tool from the Chandra Interactive Analysis of Observations (CIAO) package to correct the Level 1 data for charge transfer inefficiency.
- (b) We generate a Level 2 event file applying standard filtering techniques: we select grade=0,2,3,4,6, status=0 events and filter the event file for periods of poor aspect solution using the good time interval (GTI) data.
- (c) Periods of high background count rates are occasionally present, typically due to Solar flares (Markevitch 2001). We discard these periods by constructing a light-curve of a detec-

tor region devoid of astronomical sources, using a bin length of 500 seconds. Time intervals that are in excess of the median count rate by more than 4σ are considered to be affected by high background levels, and are discarded from the dataset. This method is similar to that employed by Markevitch (2001) for the study of blank-sky fields.

(d) We extract a cluster spectrum out to a radius that encompasses 95% of the cluster counts and use the 0.7-7 keV band. X-ray images are likewise extracted in the 0.7-7 keV band, and all visible point sources are excluded.

2.1.1. Background subtraction

Background in the ACIS instrument includes detector and astronomical components (see Markevitch et al. 2003). The background is particularly time-variable in the lowest energy channels ($E \leq 0.7$ keV; Snowden et al. 1998). At the highest energies, the cluster emission decreases and the signal becomes background-dominated. For these reasons, we limit our analysis to the 0.7-7 keV range; this band includes the Fe complex lines at ~ 6.7 keV (in the rest frame) which are necessary for an accurate determination of the plasma metallicity.

We investigate the ACIS background through the analysis of two collections of blank-sky exposures (acis57D2000-01-29bkgrndN0003.fits and acisiD2000-01-29bkgrndN0002.fits) provided with the CIAO software for the purpose of background estimation. The two datasets have exposure times of respectively 54 and 450 ks. Several other blank-sky observations are available which cover the entire life span of the Chandra mission.

The ACIS instrument is comprised of 10 CCDs on the focal plane of the Chandra telescope. A layout of the ACIS instrument is shown in Fig. 1 (see the Chandra Proposer’s Observatory Guide for further details). For each of the S3, I0, I1, I2, and I3 CCDs, we select only events in the 0.7-7 keV energy range from the two blank-sky observations. The linear size of each CCD is approximately 8 arcmin. We divide each CCD into a 6x6 grid, as indicated in Fig. 1, in order to study the spatial variation of each CCD’s response.

The S3 CCD has small spatial fluctuations in the detected counts, with a standard deviation for the 36 regions that is 7.1 % of the mean. We conclude that the ACIS-S3 CCD has a flat response, and that the background can be simply estimated from a portion of the CCD which is devoid of celestial sources (e.g., the galaxy cluster or other point sources).

The situation is different for the ACIS-I CCDs. In all four ACIS-I CCDs the response increases with distance from the read-out nodes, depicted as black rectangles in Fig. 1. This gradient in the response is at the level of 25 %, and it results in a standard deviation of

about 10 % of the mean of the counts for all CCDs, as shown in Fig. 2. No such gradient is present in the S3 data, as shown in Fig. 3. Similar results were found by Markevitch (2001) using other blank-field Chandra exposures. Since the gradient and the absolute response are similar in all four ACIS-I CCDs, the background can be estimated by using any (or all) of the CCDs that are not contaminated by the cluster emission. The aimpoint of the ACIS-I observations is I3, and I0, I1 and I2 are typically free of cluster emission.

Our background estimation technique therefore consists of selecting a region devoid of astronomical sources from the same cluster observation, according to the following scheme:

- (a) If the observation is performed with the ACIS-S configuration, the background is chosen from peripheral regions of the same ACIS-S3 CCD where the cluster is detected.
- (b) If the observation uses the ACIS-I configuration, the background is chosen from the 3 CCDs (I0, I1 and I2) that are near the I3 CCD where the cluster aimpoint is located. The background region is at the same distance from the read-out nodes as the cluster. This is the case of several observations to be presented in a follow-up paper.

2.1.2. Chandra observations of Abell 611

The X-ray data were collected by the *Chandra* telescope in the ACIS-S configuration¹. Following the analysis described above, periods of high background and poor aspect solution were filtered out, resulting in a total effective exposure time of 36,114 s. Images and spectra were limited to the 0.7-7 keV range. The morphology of the X-ray emission appears very regular. In Fig. 4 we show the ACIS-S3 image of the cluster, smoothed with a Gaussian kernel of $\sigma=4$ arcsec. The blue solid circle is the region used for the spectral extraction, cross-hatched areas are the excluded regions and the blue dashed circles are the regions used for background determination. Among the excluded regions is the cD galaxy 2MASX J08005684+3603234. The X-ray background level was 0.31 counts cm⁻² acmin⁻².

2.2. Interferometric SZE data

The SZE measurements discussed in this paper were obtained by outfitting the 6-element OVRO millimeter array in Big Pine, CA with centimeter wavelength receivers. Our receivers use coupled High Electron Mobility Transfer (HEMT) amplifiers operating in the 26-36 GHz band, with receiver temperatures $T_{rx} \sim 11$ -20 K. When combined with the OVRO system,

¹Observation took place between Nov. 3-4 2001, observation ID was 3194.

these receivers yield typical system temperatures scaled to above the atmosphere of $T_{sys} \sim 45$ K. Most of the telescopes in the array are placed in a compact configuration to maximize the sensitivity on the angular scale of distant galaxy clusters (~ 1 arcmin), but we also place a subset of the telescopes on longer baselines for simultaneous detection (and subsequent removal) of background point sources. The SZE data are reduced using the MMA software package (Scoville et al. 1993). Abell 611 was observed with the OVRO array for a total of 57 hours. No point sources were found in the field of view. In Fig. 5 we show a contour plot of the SZE data overlaid on the Chandra X-ray image. Further information on the Abell 611 OVRO data are reported in Reese et al. (2002).

3. Obtaining cluster distances

We model the spatial distribution of the cluster plasma using a β -profile, following Cavaliere and Fusco-Femiano (1976,1978):

$$n_e(r) = n_{e0} \left(1 + \frac{r^2}{r_c^2} \right)^{-\frac{3\beta}{2}} \quad (1)$$

where n_e is the electron number density, r is the radius from the cluster's center, r_c is the core radius and β is a power-law index. With this model, the thermodynamic SZE temperature decrement/increment ΔT is

$$\Delta T = f_{(x,T_e)} T_{CMB} D_A \int d\zeta \sigma_T n_e \frac{k_B T_e}{m_e c^2} = \Delta T_0 \left(1 + \frac{\theta^2}{\theta_c^2} \right)^{\frac{1-3\beta}{2}} \quad (2)$$

where $f_{(x,T_e)}$ is the frequency dependence of the SZE with $x = \frac{h\nu}{k_B T_{CMB}}$ (e.g., Reese et al. 2002 and references therein), D_A is the cluster angular diameter distance, $T_{CMB}=2.728$ K (Fixsen et al. 1996), θ is the angular radius in the plane of the sky, θ_c the corresponding angular core radius, σ_T is the Thomson cross section, k_B is Boltzmann's constant, c is the speed of light in vacuo, m_e is the electron's mass and T_e the electron's temperature. The integration is performed along the line of sight, l , and we define $\zeta = l/D_A$.

The X-ray surface brightness is given by

$$S_X = \frac{1}{4\pi(1+z)^4} D_A \int d\zeta n_e n_H \Lambda_{eH} = S_{X0} \left(1 + \frac{\theta^2}{\theta_c^2} \right)^{\frac{1-6\beta}{2}} \quad (3)$$

where S_X is the surface brightness in cgs units ($\text{ergs s}^{-1} \text{cm}^{-2} \text{arcmin}^{-2}$), z is the cluster's redshift, n_H is the plasma's hydrogen number density and $\Lambda_{eH} = \Lambda_{eH}(T_e, A)$ is the X-ray

cooling function of the gas. The cooling function is measured in the cluster’s rest frame in cgs units ($\text{erg cm}^3 \text{s}^{-1}$) integrated over the redshifted *Chandra* 0.7-7 keV band, and depends on both the electron temperature T_e and the metal abundance A . The factor $(1+z)^4$ is required for relativistic invariance.

Eq. 2 and 3 can be combined to determine D_A . Since $n_H = n_e \frac{\mu_e}{\mu_H}$,

$$D_A = \frac{\Delta T_0^2}{S_{X0}} \left(\frac{m_e c^2}{k_B T_{e0}} \right)^2 \frac{\Lambda_{eH0} \mu_e / \mu_H}{4\pi f_{(x,T_e)}^2 T_{CMB}^2 \sigma_T^2 (1+z)^4 \theta_c} \frac{1}{\left[\frac{\Gamma(3\beta/2)}{\Gamma(3\beta/2 - 1/2)} \right]^2} \frac{\Gamma(3\beta - 1/2)}{\Gamma(3\beta)} \quad (4)$$

where $\Gamma()$ is the gamma function which comes from the integration of the β -model along the central line of sight. Similarly, one can eliminate D_A to obtain n_{e0} (e.g., Reese et al. 2002; Birkinshaw 1999).

4. Joint SZE and X-ray data modelling

The SZE and the X-ray emission both depend on the properties of the hot cluster plasma. We use a joint model for the interferometric SZE radio data and the *Chandra* X-ray data which describes all the relevant spatial and spectral characteristics necessary for the distance measurement. The model consists of:

- (a) A β -model of the plasma distribution (see Eq. 2 and 3).
- (b) A photoabsorbed optically-thin spectral model (Raymond-Smith and WABS models in XSPEC) to determine T_e and A of the gas. Metal abundances are from Feldman (1992). The cluster plasma is assumed to be isothermal.
- (c) Additional parameters such as the location and flux of radio point sources and X-ray background levels.

In summary, the model is described by a set of parameters $\boldsymbol{\theta} \equiv (\beta, r_c, \Delta T_0, S_{X0}, T_e, A, \alpha)$, where α summarizes all the auxiliary parameters such as the point source location and flux, and the other parameters are used for the calculation of D_A as per Eq. 4. For each parameter set $\boldsymbol{\theta}$, we calculate the joint likelihood \mathcal{L} (e.g., Bevington 1969) of the model with the available data. Since the datasets (SZE and X-ray) are independent, the joint likelihood is the product of the individual likelihoods.

Calculation of the likelihood is a computationally intensive task. The interferometric SZE data provide constraints in the Fourier u-v plane, and the likelihood of the SZE dataset is therefore directly calculated in u-v coordinates (see Reese et al. 2000). The likelihood of the X-ray images is calculated pixel by pixel. For the spectral X-ray data, an analytical model of the emissivity (available through the XSPEC software) is convolved with the Chandra response, and the likelihood is calculated in each spectral channel.

Best-fit values and confidence intervals of the parameters θ can be obtained through likelihood ratio methods, as in Reese et al. (2002). In this paper, we employ an alternative Monte Carlo Markov chain method, which is more efficient than the traditional likelihood ratio methods.

4.1. The Monte Carlo Markov chain method applied to Abell 611

A Monte Carlo Markov chain (MCMC) is a sequence of model parameters θ . Each parameter $\theta_i \in \theta$ can vary within two limiting values and values of each parameter θ_i appear in the MCMC with a frequency that is determined by the parameter’s true probability distribution (Gilks, Richardson and Spiegelhalter 1996).

A MCMC is constructed by drawing candidates θ' from the parameter space. Each candidate is rejected or accepted in the chain according to an acceptance criterion which uses the likelihood information. The criterion we employ is the Metropolis-Hastings algorithm (Metropolis et al. 1953; Hastings 1970; Gilks, Richardson and Spiegelhalter 1996). If the parameters are accepted, a link is added to the chain and $\theta_{n+1} = \theta'$; if the parameters are rejected, the chain remains at its previous location, and $\theta_{n+1} = \theta_n$.

A proper choice for the support of each parameter $\theta_i \in \theta$ is very important. A large support allows the chain to investigate many candidate θ_i ; however, it oftentimes results in a very low acceptance rate, as most of the candidates are rejected because of their poor likelihood. The hard limits imposed on each parameter were therefore determined by test runs of the Markov chain (with typically 1,000-10,000 steps) to ensure that the chosen support did not exclude any interesting regions in parameter space. Table 1 shows the hard limits used for the MCMC of Abell 611 ².

In constructing a MCMC one has the freedom to choose any desired method for drawing candidates (Roberts 1996). We draw candidates θ' that are in the neighborhood of the previously accepted parameters, instead of drawing them from the full parameter space. Our ‘proposal’ distribution is therefore a top-hat function with a width of 25 % of the parameter’s support (see Table 1). A small width for the proposal distribution typically results in a high acceptance rate, as candidates have a likelihood that is similar to that of the previously accepted parameters. On the other hand, a large number of steps is required

²To test the goodness of our choice, we also ran another Markov chain following the specifications of Table 1 but without enforcing the hard limits. The results (not shown) were indistinguishable from those of the Markov chain featuring the hard limits.

for the Markov chain to scan the entire parameter space.

The starting point of a Markov chain can be chosen arbitrarily (Gilks, Richardson and Spiegelhalter 1996). We start the Markov chain at the midpoint of each parameter’s support (see Table 1). The chain was run for 100,000 iterations, and it resulted in an acceptance rate of 10.4%. In Fig. 6 we show the initial 2000 steps for the parameters S_X and D_A .

4.2. Convergence of the Markov chain

A Markov chain requires a given number of steps before it reaches convergence. We test the convergence of the MCMC by means of the Geweke test (Geweke 1992; Gamermann 1997; Geyer 1992), which is based on the comparison between the initial and final segments of the chain.

We discard the initial $n_i=5,000$ steps of the chain (the *burn-in* period), and divide the remaining $n=95,000$ steps into the initial 10% ($n_b = 9,500$) and the final 40% ($n_a = 38,000$) segments, according to Geweke (1992). The intermediate 40% portion is not used for testing the convergence.

Since the values in the Markov chain are correlated by construction, the initial and final segments are averaged over $m=100$ steps, to ensure that the rebinned values are uncorrelated (Roberts 1996). After rebinning, the initial segment has a length of $n'_b = 9,500/100 = 95$ and the final segment has a length of $n'_a = 38,000/100 = 380$ steps. The batch means for each parameter θ_i during the initial and final segments are respectively:

$$\overline{\psi_{b,i}} = \frac{1}{n'_b} \sum_{j=n'_i}^{n'_i+n'_b} \overline{\theta_i(j)} \qquad \overline{\psi_{a,i}} = \frac{1}{n'_a} \sum_{j=n'-n'_a}^{n'} \overline{\theta_i(j)} \qquad (5)$$

where $n' = n/m = 95,000/100 = 950$, $n'_i = n_i/m = 5,000/100 = 50$ and $\overline{\theta_i}$ indicates the parameter average over the m steps.

The standardized difference between the initial and the final portions of the chain for each parameter is then given by

$$z_{G,i} = \frac{\overline{\psi_{a,i}} - \overline{\psi_{b,i}}}{\sqrt{Var(\overline{\psi_{a,i}}) + Var(\overline{\psi_{b,i}})}} \qquad (6)$$

The z_G function, also known as the Geweke z-score, is distributed as a standard Gaussian $N(0,1)$, and therefore convergence is indicated if values of z_G are less than ~ 3 for all

parameters (Geweke 1992; Gamerman 1992). The z_G values for Abell 611 with a $n=95,000$ step Markov chain are shown in Table 2.

4.3. Results of the MCMC for Abell 611

In Fig. 7 we show the probability distribution of a few interesting parameters, and in Table 2 the median of the distribution of each parameter and the 68 % and 90 % confidence intervals. The median can be interpreted as the best-fit value of each parameter. Fig. 7 displays a major strength of the MCMC method: the full probability distribution of each parameter is known, without the need for a Gaussian approximation. It is clear that the probability distribution of D_A , for example, has a skewness towards large values of D_A , and it is not well represented by a Gaussian function. This represents a major improvement over likelihood ratio techniques.

4.4. Comparison with likelihood ratio methods

We employ the XSPEC spectral code to compare the confidence intervals on the spectral parameters T_e and A . Table 3 shows the comparison between the MCMC-derived best-fit values and confidence intervals with those provided by XSPEC, which uses likelihood ratio methods. The results are in excellent agreement, further corroborating the integrity of our MCMC approach. In addition, we use the CIAO Sherpa software to determine the β -model parameters, and results are also shown in Table 3. The agreement with the results of Table 2 provides additional confidence on the reliability of our analysis.

Abell 611 data were also analyzed by Reese et al. (2002) using a likelihood ratio method. They found a SZE decrement of $\Delta T_0 = -853 \pm_{140}^{120} \mu\text{K}$. Our results of $\Delta T_0 = -800 \pm 83 \mu\text{K}$ are again in very good agreement with theirs.

5. Conclusions

We presented a Monte Carlo Markov chain technique to derive cluster distances from SZE and X-ray data. The method was successfully tested on the OVRO and Chandra data of Abell 611, a galaxy cluster at $z=0.288$. We measure an angular diameter distance of $D_A = 0.98 \pm_{0.20}^{0.23}$ Gpc (68% confidence level). In a previous work based on the same SZE data, but using lower-resolution X-ray data, Reese et al. (2002) derived a distance of $D_A = 0.99 \pm_{0.29}^{0.32}$ Gpc.

The MCMC method has two major advantages: it provides the full probability distribution of the angular distance D_A and of all other associated physical parameters, such as the SZE decrement and the β -model parameters, and it is computationally more efficient than the traditional likelihood ratio-based methods.

This technique will be used in a follow-up paper to determine the distances of a large sample of galaxy clusters for which there are available high-resolution Chandra X-ray data and BIMA/OVRO SZE data.

REFERENCES

- Avni, Y. 1976, ApJ, 210, 642
- Baluchinska-Church, M. and McCammon, D. 1992, ApJ, 400, 699
- Bevington, P.R. 1969, Data reduction and error analysis for the physical sciences, McGraw-Hill
- Birkinshaw, M. 1999, Phys. Rep., 310, 97
- Cash, W. 1979, ApJ, 228, 939
- Cavaliere, A. and Fusco-Femiano, R. 1976, A&A, 49, 137
- Cavaliere, A. and Fusco-Femiano, R. 1978, A&A, 70, 677
- Dickey, J.M. and Lockman, F.J. 1990, ARA&A, 28, 215
- Feldman, U. 1992, Physica Scripta, 46, 202
- Fixsen, D.J. et al. 1996, ApJ, 473, 576
- Gamerman, D. 1997, Markov Chain Monte Carlo: stochastic simulation for Bayesian inference, Chapman and Hall
- Geweke, J. 1992, in Bayesian Statistics IV, Ed. Bernardo, J.M. e al., Clarendon Press-Oxford, 169
- Geyer, C.J. 1992, Practical Markov Chain Monte Carlo, Statist. Sci., 7, 473
- Gilks, W.R., Richardson, S. and Spiegelhalter, D.J. 1996, Markov Chain Monte Carlo in practice, Chapman and Hall

- Gould, R.J. 1980, ApJ, 238, 1026
- Hastings, W.K. 1970, Biometrika, 57,97
- Lampton, M., Margon, B. and Bowyer, S. 1976, ApJ, 208, 177
- Markevitch, M. 2001, CXC memo (<http://asc.harvard.edu/cal>)
- Markevitch, M. et al. 2003, ApJ, 583, 70
- Metropolis, N., Rosenbluth, A.W., Rosenbluth, M.N., Teller, A.H. and Teller, E. 1953, Journal of Chemical Physics, 21, 1087
- Morrison, R. and McCammon, D. 1983, ApJ, 270, 119
- Narlikar, J.V. 1983, Introduction to Cosmology, Jones and Bartlett Publishers
- Pearson, T.J., Shepherd, M.C., Taylor, G.B. and Meyers, S.T. 1994, BAAS, 185, 808
- Press, S.J. 1989, Bayesian Statistics: principles, models and applications, New York:Wiley
- Raymond, J.C. and Smith, B.W. 1977, ApJS, 35, 419
- Roberts, G.O. 1996, in Markov Chain Monte Carlo in practice, Ed.s Gilks, W.R., Richardson, S. and Spiegelhalter, D.J., Chapman and Hall, 45.
- Reese, E.D. et al. 2000, ApJ, 533, 38
- Reese, E.D., Carlstrom, J.E., Joy, M.K., Mohr, J.J., Grego, L. and Holzzapfel, W.L. 2002, ApJ, 581, 53
- Scoville, N.Z. et al. 1993, PASP, 105, 1482
- Snowden, S.L., Egger, R., Finkbeiner, D.P., Freyberg, M.J. and Plucinsky, P.P. 1998, ApJ, 493, 715
- Sunyaev, R.A. and Zeldovich, Y.B. 1970, Comments Astrophys. Space Phys., 2, 66
- Sunyaev, R.A. and Zeldovich, Y.B. 1972, Comments Astrophys. Space Phys., 4, 173
- Wilms, J., Allen, A. and McCray, R. 2000, ApJ, 542, 914

Table 1. MCMC model parameters for Abell 611 data

Parameter	Min. value	Max value	Starting value	Units
S_X	32	42	37	counts/cm ² /arcmin ²
r_c	17	23	20	arcsec
β	0.56	0.62	0.059	–
ΔT_0	-1.20	-0.60	-0.90	mK
$K_B T_e$	4.5	8	6.25	keV
A	0.05	0.5	0.275	solar

Note. — Units for S_X (and the background level) can be converted to the more physical units of counts/s/arcmin² by multiplying the numbers times the S3 effective area (603 cm² for this observation) and dividing by the exposure time (36,114 s for this observation).

Table 2. MCMC results for Abell 611 data

Parameter	Median	68 % interval	90 % interval	z_G
S_X	36.9	$\pm_{1.1}^{1.1}$	$\pm_{1.7}^{1.9}$	-0.63
r_c	20.00	$\pm_{0.65}^{0.68}$	± 1.10	0.47
β	0.594	$\pm_{0.007}^{0.008}$	$\pm_{0.012}^{0.013}$	0.21
ΔT_0	-0.800	$\pm_{0.083}^{0.082}$	$\pm_{0.136}^{0.133}$	-0.77
$k_B T_e$	6.23	$\pm_{0.29}^{0.29}$	$\pm_{0.46}^{0.49}$	0.26
A	0.25	$\pm_{0.05}^{0.05}$	$\pm_{0.08}^{0.09}$	-0.51
Λ_{eH}	2.19	$\pm_{0.026}^{0.026}$	$\pm_{0.042}^{0.041}$	-0.33
D_A	0.98	$\pm_{0.20}^{0.23}$	$\pm_{0.31}^{0.40}$	0.81

Table 3. Comparison of MCMC results with XSPEC and CIAO Sherpa results

Parameter	68% interval (MCMC)	68% interval (XSPEC/Sherpa)
$k_B T_e$	$6.23 \pm_{0.29}^{0.29}$	6.20 ± 0.30 (XSPEC)
A	0.25 ± 0.05	0.25 ± 0.05 (XSPEC)
S_X	$36.9 \pm_{1.1}^{1.1}$	$38.5 \pm_{1.2}^{1.1}$ (Sherpa)
r_c	$20.00 \pm_{0.65}^{0.68}$	19.42 ± 0.63 (Sherpa)
β	$0.594 \pm_{0.007}^{0.008}$	0.589 ± 0.01 (Sherpa)

Note. — The CIAO Sherpa spatial fit is based only on the Chandra X-ray data, not the combination of X-ray and radio data, as in Table 2. We determined, however, that the results of Table 2 are virtually unchanged when the X-ray data alone are used for the determination of the beta model; the high S/N X-ray data drive the fit of the spatial parameters.

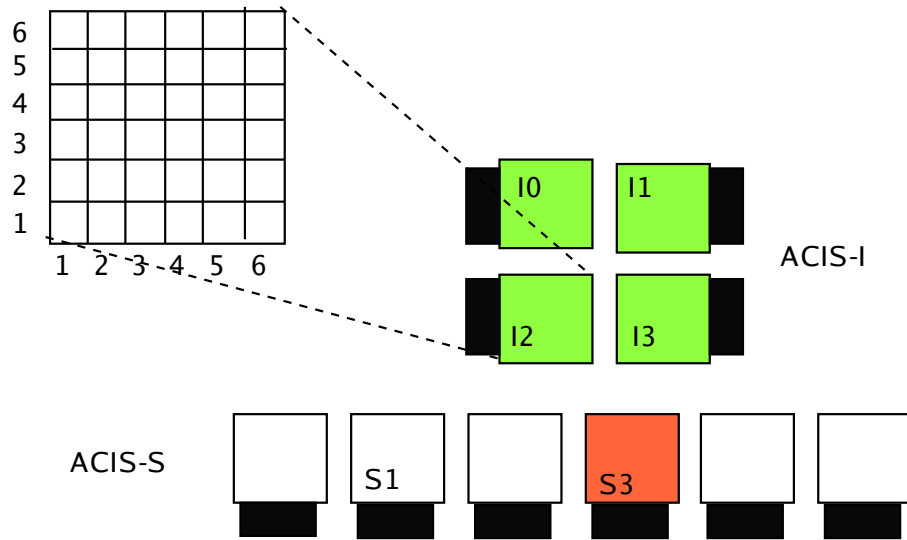


Fig. 1.— Layout of the ACIS detector, not to scale. Each CCD is divided into 36 zones to study the spatial behavior of the response. Black rectangles represent the read-out nodes of each CCD

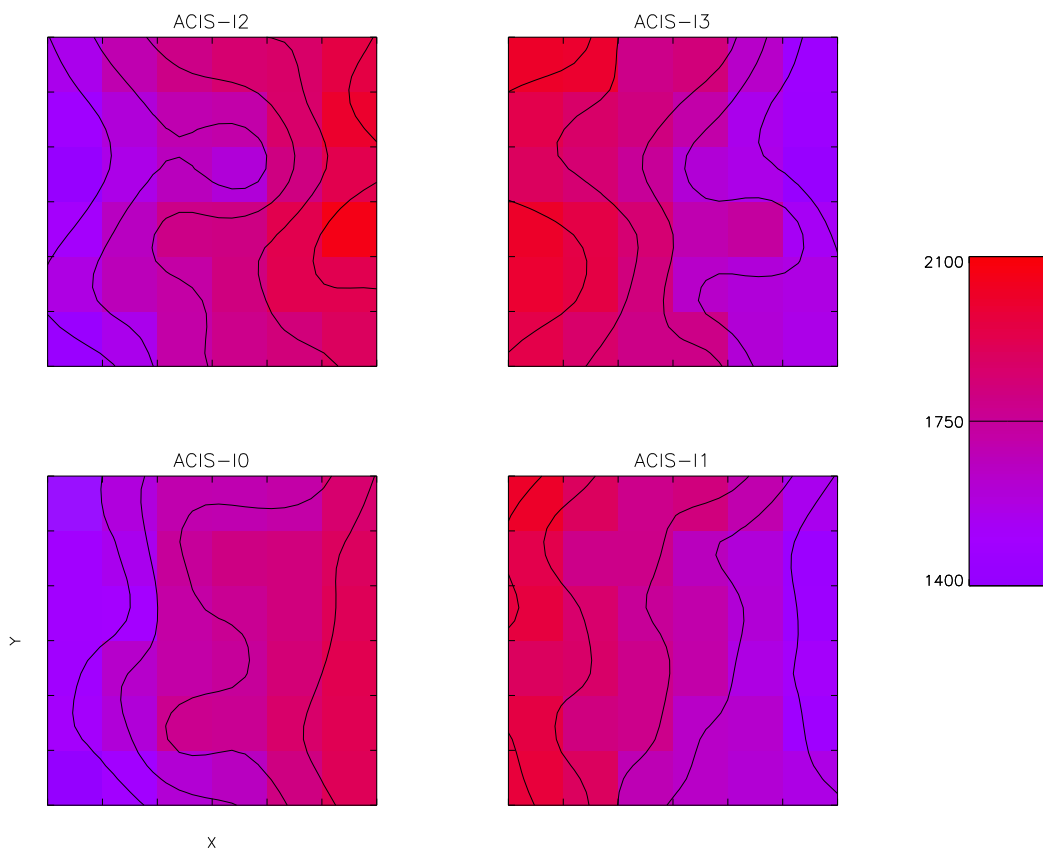


Fig. 2.— Spatial behavior of the ACIS-I response in 0.7-7 keV band. Counts from the 450 ks blank-field exposure (see text for details) were accumulated in $\sim 1.4 \times 1.4$ square arcmin pixels.

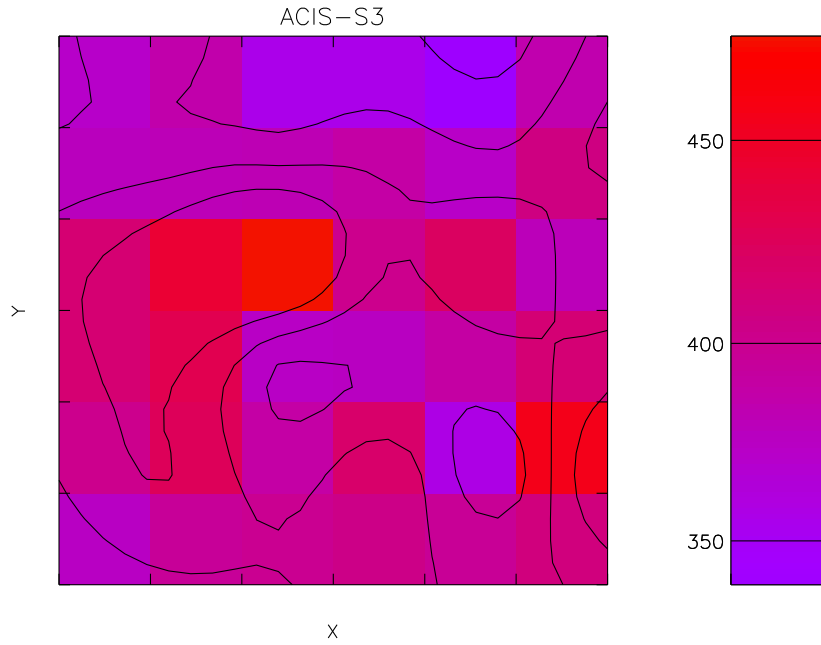


Fig. 3.— Spatial behavior of the ACIS-S3 response in 0.7-7 keV band. Counts from the 54 ks blank-field exposure (see text for details) were accumulated in $\sim 1.4 \times 1.4$ square arcmin pixels.

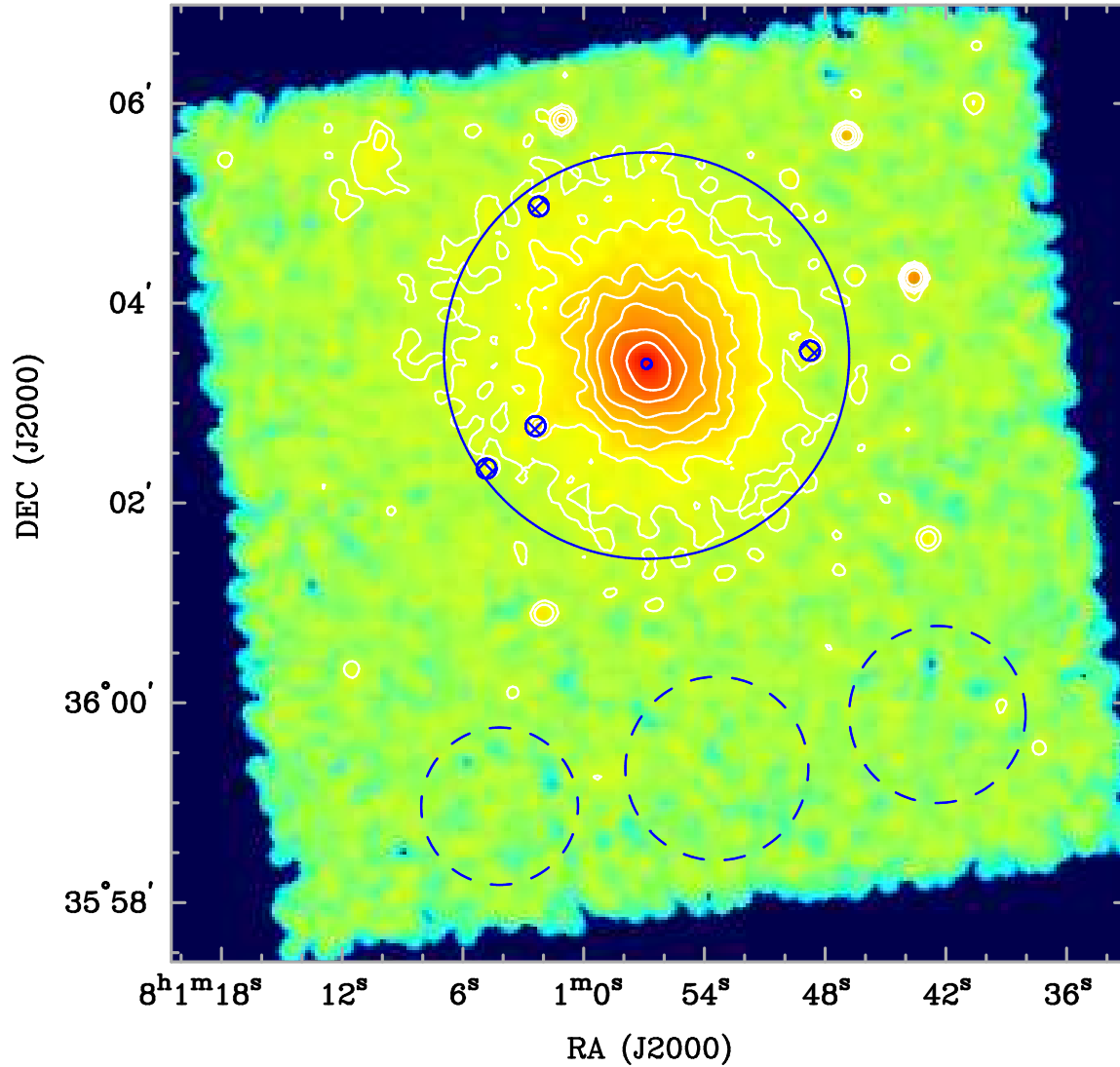


Fig. 4.— Chandra 0.7-7 keV image of Abell 611. Image is not exposure corrected, contours are 0.5, 1, 2, 3, 5, 9 and 15 counts/pixel, pixel size is 1.97 arcsec. The image was smoothed with a Gaussian kernel of $\sigma=4$ arcsec. The solid circle encompasses 95% of the cluster counts, cross-hatched areas were excluded because contaminated by point sources. Dashed circles are the regions used for background determination.

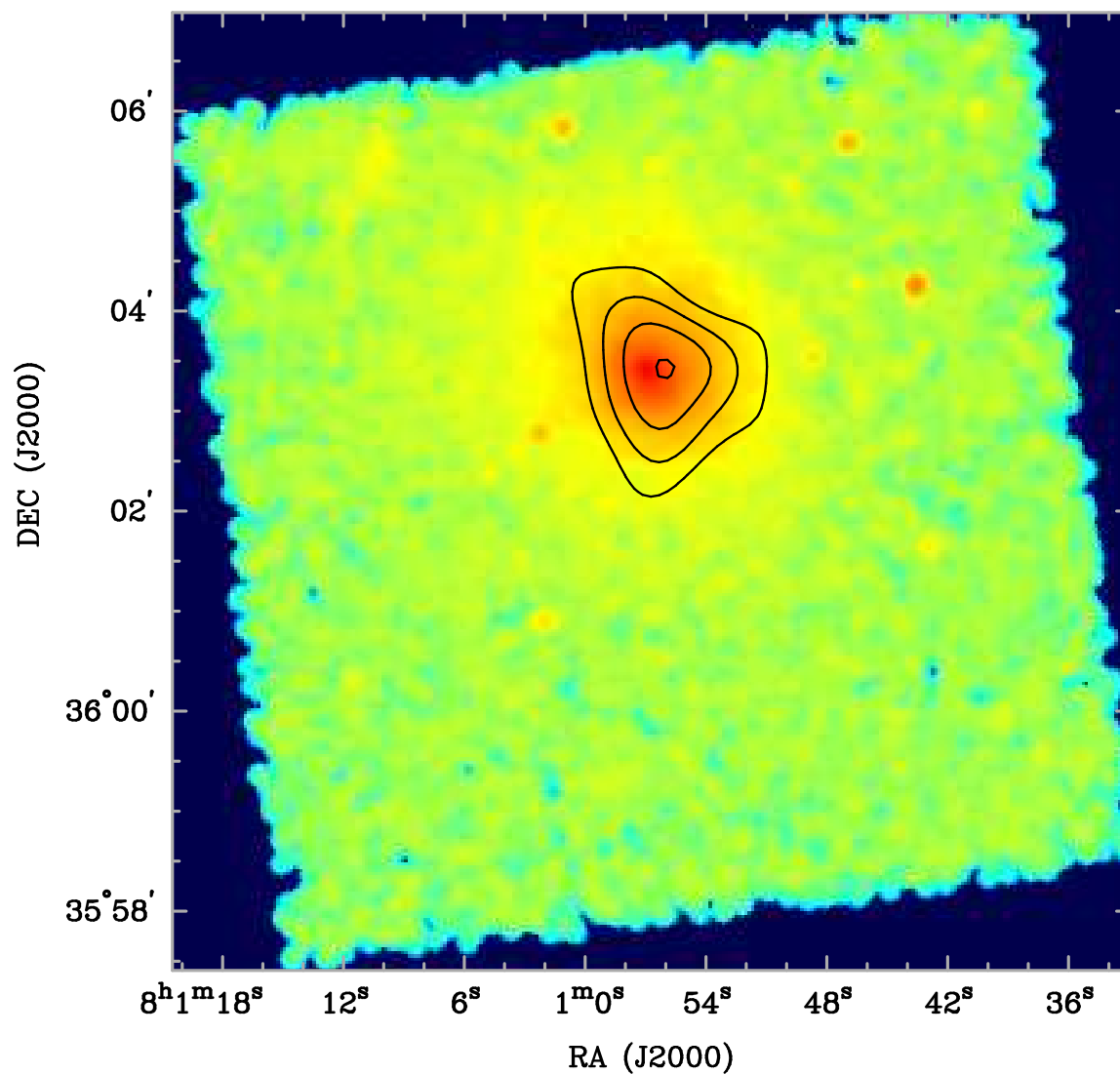


Fig. 5.— SZE contours overlaid on the Chandra 0.7-7 keV image of Abell 611. The contours are -4 , -3 , -2 and -1×10^{-4} mJ/beam.

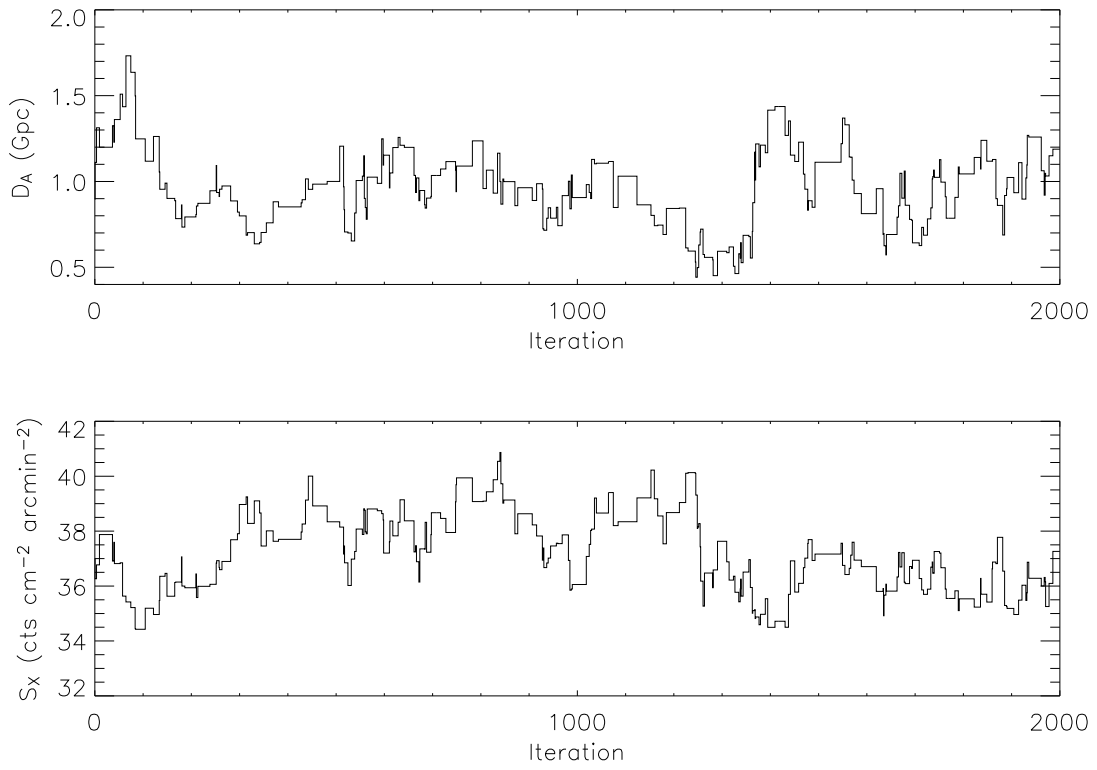
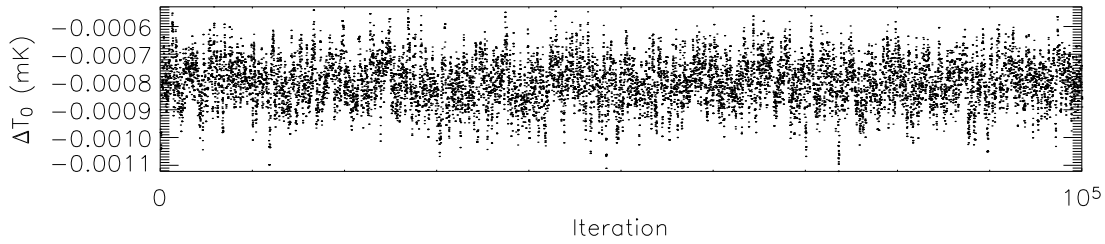
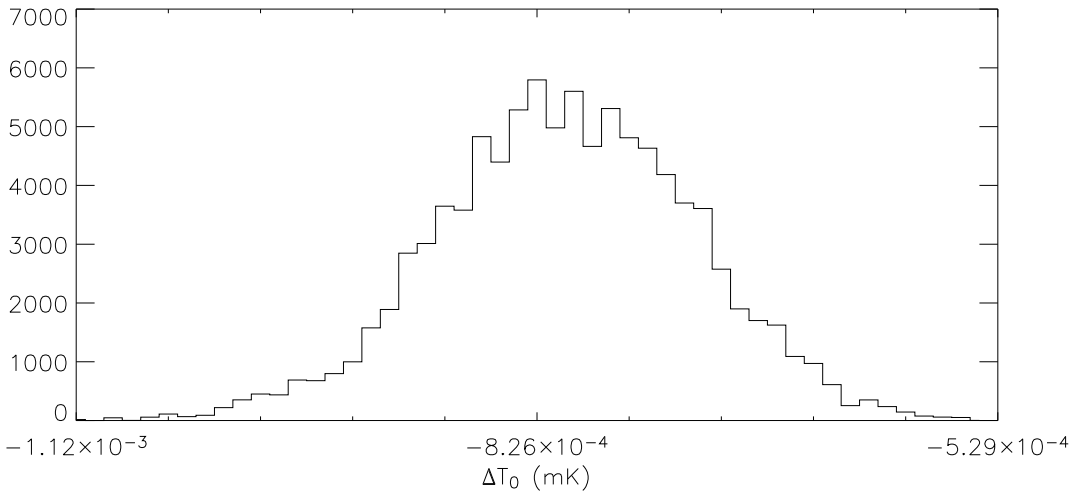
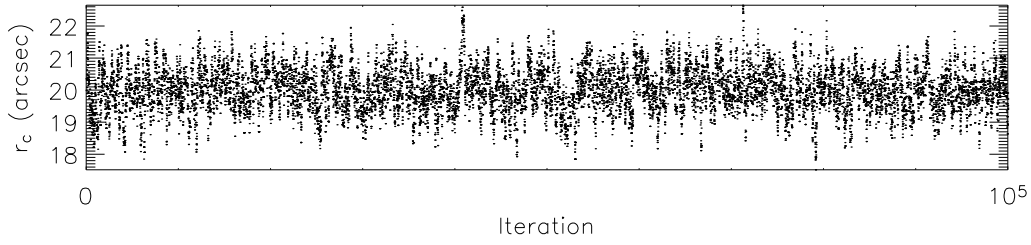
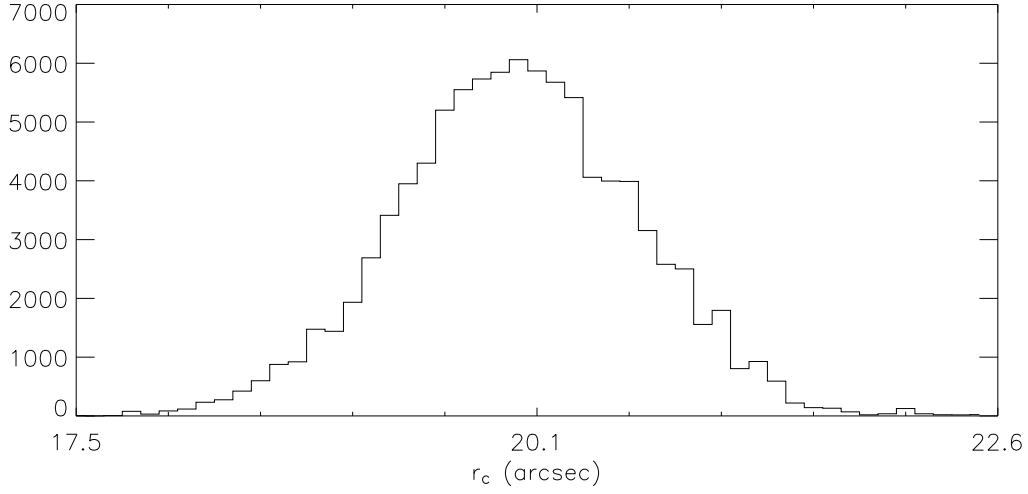


Fig. 6.— Initial 2,000 iterations of the Markov chain for parameters D_A and S_X (see Table 1 for units of measure).



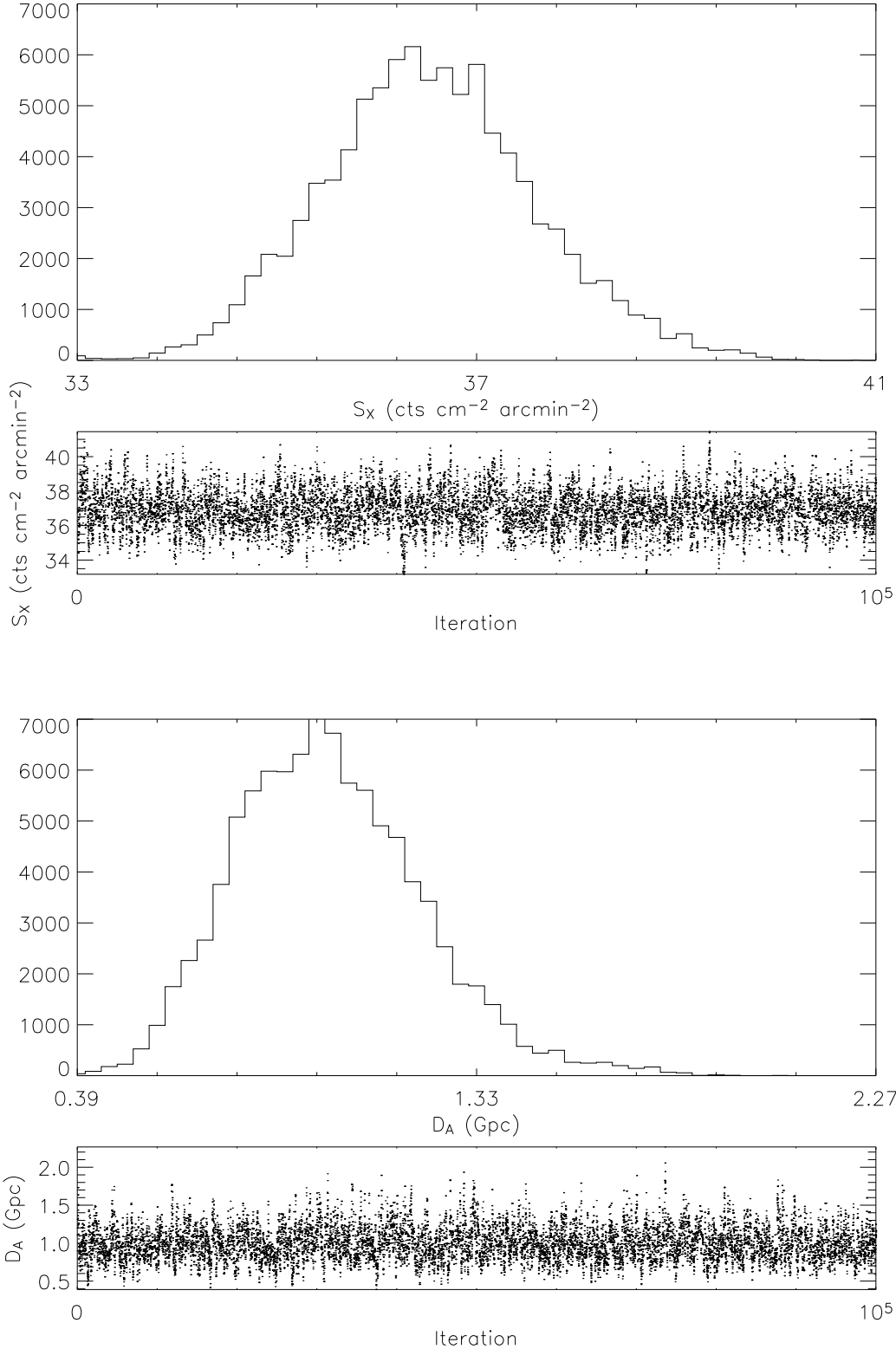


Fig. 7.— Results of the Markov chain for 4 of the 8 parameters of interest, r_c , ΔT_0 , S_X and D_A . Top: probability distribution. We excised the initial 5,000 events, and used 95,000 events to determine the distribution. Bottom: time series of the Markov chain including all